Marine and Petroleum Geology 27 (2010) 748–756

Contents lists available at ScienceDirect

Marine and Petroleum Geology

journal homepage: www.elsevier.com/locate/marpetgeo

Authigenic carbonates from methane seeps of the northern Congo fan: Microbial formation mechanism

Dong Feng [a], Duofu Chen [a,*], Jörn Peckmann [b], Gerhard Bohrmann [b]

[a] CAS Key Laboratory of Marginal Sea Geology, Guangzhou Institute of Geochemistry, Chinese Academy of Sciences, Guangzhou 510640, China
[b] MARUM, University of Bremen, Post Box 330 440, D-28334 Bremen, Germany

ARTICLE INFO

Article history:
Received 15 May 2009
Received in revised form
25 July 2009
Accepted 17 August 2009
Available online 22 August 2009

Keywords:
Methane
Seep
Carbonate
Isotopes
Rare earth elements
Trace elements
Seepage rate
Congo fan

ABSTRACT

Authigenic carbonates were collected from methane seeps at Hydrate Hole at 3113 m water depth and Diapir Field at 2417 m water depth on the northern Congo deep-sea fan during RV Meteor cruise M56. The carbonate samples analyzed here are nodules, mainly composed of aragonite and high-Mg calcite. Abundant putative microbial carbonate rods and associated pyrite framboids were recognized within the carbonate matrix. The $\delta^{13}C$ values of the Hydrate Hole carbonates range from −62.5‰ to −46.3‰ PDB, while the $\delta^{13}C$ values of the Diapir Field carbonate are somewhat higher, ranging from −40.7‰ to −30.7‰ PDB, indicating that methane is the predominant carbon source at both locations. Relative enrichment of ^{18}O ($\delta^{18}O$ values as high as 5.2‰ PDB) are probably related to localized destabilization of gas hydrate. The total content of rare earth elements (REE) of 5% HNO_3-treated solutions derived from carbonate samples varies from 1.6 ppm to 42.5 ppm. The shale-normalized REE patterns all display positive Ce anomalies ($Ce/Ce^* > 1.3$), revealing that the carbonates precipitated under anoxic conditions. A sample from Hydrate Hole shows a concentric lamination, corresponding to fluctuations in $\delta^{13}C$ values as well as trace elements contents. These fluctuations are presumed to reflect changes of seepage flux.

1. Introduction

Carbonate precipitation is a widely observed phenomenon in modern and ancient marine seep environments (e.g. Roberts and Aharon, 1994; Peckmann and Thiel, 2004; Campbell, 2006; Naehr et al., 2007). It is a product of anaerobic oxidation of methane (AOM), which is mediated by consortia of methane-oxidizing archaea (MOA) and sulfate-reducing bacteria (SRB; Hinrichs et al., 1999; Boetius et al., 2000). Bicarbonate released during AOM increases alkalinity and results in the precipitation of authigenic carbonate (cf. Berner, 1980). Accordingly, the study of stable isotopes, lipid biomarkers, and biogenic fabrics of seep carbonates provides further insight into microbially mediated carbonate formation (e.g. Roberts and Aharon, 1994; Thiel et al., 1999; Boetius et al., 2000; Peckmann et al., 2001; Peckmann and Thiel, 2004; Pape et al., 2005; Chen et al., 2005, 2006, 2007; Campbell, 2006; Birgel and Peckmann, 2008; Feng et al., 2008). Furthermore, stable carbon and oxygen isotopic compositions of carbonates provide information pertaining to the composition and temperature of seep fluids from which carbonates precipitated (e.g. Naehr et al., 2000, 2007; Peckmann and Thiel, 2004).

The relative upward fluid flux at seep sites may change over time (Roberts and Carney, 1997; Roberts, 2001; Hovland, 2002; Chen et al., 2004; Lapham et al., 2008) and this temporal variability can be expressed by different geochemical and mineralogical signatures archived in authigenic seep carbonates (León et al., 2007; Feng et al., 2009a,b). For example, De Boever et al. (2006a,b) pointed out that carbon isotopes can be used to assess the control of seepage rates on the formation of ancient seep carbonates. However, only relatively few studies have used such an approach due to the scarcity of appropriate samples.

During AOM, sulfate in pore water is reduced to hydrogen sulfide (Valentine and Reeburgh, 2000). As a consequence of sulfate-dependent methane oxidation, redox conditions in the sediment at seeps change. Cerium is a sensitive indicator of redox conditions in sedimentary environments. Under oxidizing conditions Ce^{3+} is oxidized to Ce^{4+}, and precipitates as CeO_2, resulting in a negative Ce anomaly, which is therefore an effective indicator of oxic conditions (McArthur and Walsh, 1984; Wright et al., 1987). Negative Ce anomalies in marine carbonates have been shown to reflect seawater oxygenation (McArthur and Walsh, 1984; Sholkovitz and

* Corresponding author. Tel.: +86 20 85290286; fax: +86 20 85290130.
E-mail addresses: fd@gig.ac.cn (D. Feng), cdf@gig.ac.cn (D. Chen), peckmann@uni-bremen.de (J. Peckmann), gbohrmann@uni-bremen.de (G. Bohrmann).

0264-8172/$ – see front matter © 2009 Elsevier Ltd. All rights reserved.
doi:10.1016/j.marpetgeo.2009.08.006

Shen, 1995; Shields and Webb, 2004). Trace elements, such as V, Mo, U, and Cd are also redox sensitive elements that are enriched under anoxic conditions (Morford and Emerson, 1999). Thus, REE and trace elements can be used to illuminate the formation conditions of authigenic carbonate phases.

Here, we present a study of authigenic seep carbonates from two locations (Hydrate Hole and Diapir Field) of the Congo deep-sea fan (Fig. 1). The mineralogy, petrography, stable carbon and oxygen isotope compositions were studied along with rare earth elements (REE) and trace elements to evaluate the role and mode of microbial activity in the precipitation of seep carbonates and the dynamics of seepage over the course of carbonate formation.

2. Geological setting

The lower Congo basin is one of the numerous sub-basins of the West African passive margin that developed during the opening of the southern Atlantic Ocean during the Early Cretaceous (Marton et al., 2000). In the Early Aptian up to 1000 m thick salt-deposits accumulated, which were subsequently buried by black shale and bituminous sandstones in the Late Aptian (Uenzelmann-Neben, 1998). Increased terrigenous sediment input to the Atlantic Ocean during the Cenozoic resulted in the initiation of the turbiditic sedimentation system along the western African margin. Terrigenous material from the Congo river was transported through the Congo canyon to the deep Angola basin and deposited as a 2000–3000 m thick delta on the continental shelf and slope (Droz et al., 1996; Gay et al., 2006a). Updip migration of deeper thermogenic fluids resulted in the preferential trapping of oil and gas in these coarse-grained, paleo-channel-filling sediments, which now serve as hydrocarbon reservoirs (Gay et al., 2006b and references therein).

An area with several pockmarks was identified by detailed seismic and echo-sound profiles on the Congo deep-sea fan during cruises M47 and M56 with RV Meteor (Sahling et al., 2008). The so-called "Kouilou pockmarks" range from several tens to hundreds of meters in diameter and a few to tens of meters in depth. They include three large, individual pockmarks, namely "Worm Hole", "Hydrate Hole", and "Black Hole". Hydrates were found at sediment depth below ~50 cm up to the maximum gravity corer sampling depth of 12 m from all three pockmarks. It is very probable that additional gas hydrates exist below that depth (Sahling et al., 2008).

3. Materials and methods

Abundant authigenic carbonates are found close to the sediment surface of the northern Congo fan pockmark area (Sahling et al., 2008). The carbonate nodules analyzed in this study were collected by TV-guided grabs from two sites previously named Hydrate Hole and Diapir Field during RV METEOR Cruise M56 (Table 1). Three samples collected from Hydrate Hole at approximately 3113 m water depth, and one sample collected from Diapir Field at approximately 2417 m water depth are analyzed in this study (Fig. 1). Living vestimentiferan tube worms and various bivalves are present at the two sampling sites (Sahling et al., 2008; Haas et al., 2009). Samples were dried after collection and subsequently cut into sections for sub-sampling, thin section preparation, scanning electron microscopy (SEM), X-ray diffraction (XRD), stable carbon and oxygen isotope measurements, and REE as well as trace element analyses. Subsamples for the isotope and element analyses were taken from slabs with a computer-assisted microsampling device (MicroMill, New Wave Research).

Petrographic observations of thin sections of the samples were made using a LEICA-DMRX optical microscope. Carbonate microstructure of external surfaces and surfaces resulting from the breaking of samples was examined with a field emission scanning electron microscope (FE-SEM). The samples were prepared by gold coating to a thickness of approximately 20 nm. Photographs were taken with a Sirion 200 FE-SEM equipped with EDAX GENESIS at Central South University (CSU), operating at 10–20 kV at 5–9 mm working distance. For XRD, the samples were crushed to powder less than 200 mesh using an agate mortar and pestle. The analyses were performed at CSU using a Rigaku DXR 3000 computer-automated diffractometer utilizing Bragg-Brentano geometry. The X-ray source was a Cu anode operated at 40 kV and 40 mA using CuKα radiation equipped with a diffracted beam graphite monochromator. The

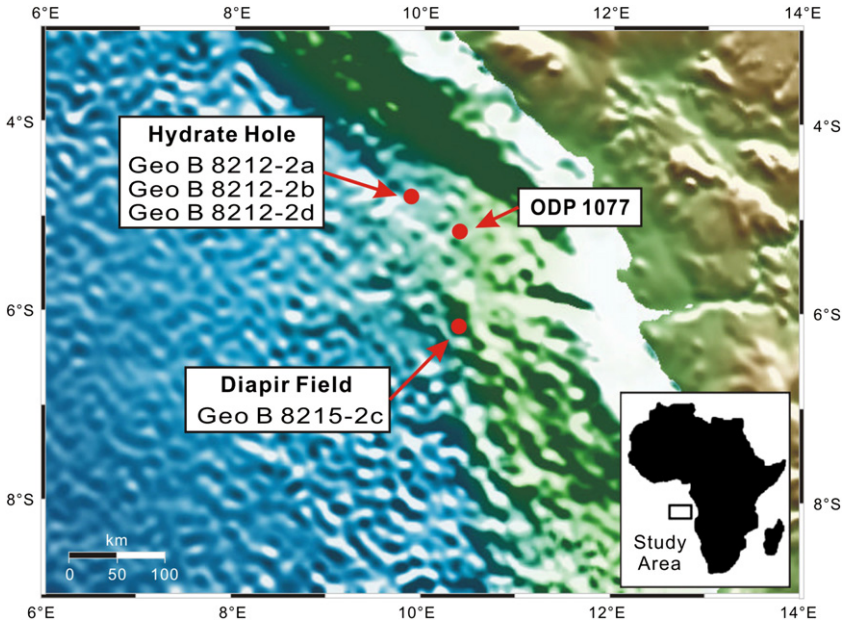

Fig. 1. Locations of the studied sites modified after R/V Meteor Cruise M56 Report and Preliminary Results (http://www.marinegeo.uni-bremen.de/pub). Hydrate Hole is 04°48′56″S/09°54′50″E, and Diapir Field is 06°11′04″S/10°25′53″E.

Table 1
Site information and mineral composition of the Congo deep-sea fan seep carbonates.

Location	Sample number	Water depth (m)	Approximate relative percentages (wt. %)					
			Aragonite	Calcite	High-Mg Calcite	Kaolinite	Quartz	Barite
Hydrate Hole	GeoB 8212-2a	3113	89.6	2.6	–	4.6	–	3.1
	GeoB 8212-2b	3113	17.0	–	74.3	5.3	3.4	–
	GeoB 8212-2d	3113	7.9	–	89.6	1.5	1.0	–
Diapir Field	GeoB 8215-2c	2417	68.1	–	29.6	1.3	1.0	–

orientated samples were scanned at an interval of 5–65° (2θ) with a step size of 0.02° and a count time of 5 s per step. Divergence, scattering, and receiving slits were 0.5°, 0.5° and 0.15 mm, respectively. Relative abundance of the minerals was semi-quantified by Rietveld analysis of the diffractograms with the program SIROQUANT (Taylor, 1991).

The powdered samples were processed with 100% phosphoric acid to release CO_2 for stable carbon and oxygen isotope analysis using a GV Isoprime II stable isotope mass spectrometer. All isotope values are expressed using the δ-notation relative to the PeeDee Belemnite (PDB) standard and are reported in permil (‰) with a standard deviation of less than 0.1‰ (2σ) for both $\delta^{18}O$ and $\delta^{13}C$ values.

We analyzed 5% HNO_3-treated solutions obtained from authigenic carbonate minerals for REE and trace elements. The powder samples (~0.5 g) were treated with 50 ml of 5% HNO_3 in a centrifuge tube for 2–3 h to separate carbonate mineral and residue phases. Then, 2500 ng of rhodium was added as an internal standard for calculating the element concentration of the dissolved carbonate mineral phase. Five milliliters of this solution were further diluted 10 times for the REE analysis using a Finnigan MAT ELEMENT high resolution ICP-MS. For detail of the analyses see Qi et al. (2005). Precision of the REE analysis was checked by multiple analyses of standard samples. The average standard deviations are less than 10%, and average relative standard deviations are better than 5%. For reliability of the analyses, see Chen et al. (2005). In this paper, Ce/Ce* denotes $3Ce_N/(2La_N + Nd_N)$, Ce_{anom} denotes Log (Ce/Ce*), and Pr/Pr* denotes $2Pr_N/(Ce_N + Nd_N)$, where N refers to normalization of concentration against the standard Post Archean Australian Shale (PAAS; McLennan, 1989).

4. Results

4.1. Mineralogy and petrography

The XRD results reveal that the carbonate samples are mainly a mixture of aragonite and high-Mg calcite (HMC) (Table 1), although pure aragonite is also present. Aragonite forms crusts (Fig. 2A) and fills worm tubes (Fig. 2B). It occurs both as microcrystalline cement and as fibrous crystals forming isopachous rims (Figs. 2–4). Micritic HMC is the dominant mineral in two of the samples (GeoB 8212-2b and GeoB 8212-2d), in which aragonite was found only as fibrous pore-filling cement (Figs. 2B and 3A). All samples contain minor kaolinite and quartz except for sample GeoB 8212-2a. Low-Mg calcite (LMC) and barite occur as trace minerals only in sample GeoB 8212-2a, which is rich in aragonite. Since barite is known to form at the sulfate–methane interface (Castellini et al., 2006), its presence suggests that the sulfate–methane interface at the studied site was shallow during mineral formation. Aragonite precipitation is favored in the presence of sulfate-rich pore fluids close to the seafloor. Pyrite framboids, approximately 5–20 μm in diameter, are dispersed within the microcrystalline matrix of the samples and frequently occur within foraminiferal tests (Figs. 2 and 4). Micropores, generally less than 0.5 mm in diameter are common (Figs. 2A–C and 3D), especially in sample GeoB 8215-2c (Fig. 2C). Diatom frustules are abundant in the carbonates (Figs. 3C, 4C and F).

4.2. Stable carbon and oxygen isotopes

The $\delta^{13}C$ values of Hydrate Hole carbonate samples vary between −62.5‰ and −46.3‰, with $\delta^{18}O$ values ranging from 2.9‰ to 5.2‰ (Fig. 5). Carbonate phases of the Diapir Field sample reveal a narrower range of $\delta^{13}C$ and $\delta^{18}O$ values, from −40.7‰ to −30.7‰ and 3.4‰ to 4.8‰, respectively (Fig. 5).

In sample GeoB 8212-2a, a trend towards lower $\delta^{13}C$ and $\delta^{18}O$ values from the outer to the inner part of the aragonite rim is apparent (Fig. 6). In Fig. 7, isotope data of the concentrically zoned sample GeoB 8212-2b (Fig. 7A) are presented, which was subsampled along two mutually perpendicular transects (Fig. 7B). In total, three zones of distinct isotopic signatures can be differentiated (Fig. 7C and D). The highest $\delta^{13}C$ values correspond to a central zone (Zone I). Zone II shows the lowest $\delta^{13}C$ values. Zone III again reveals higher $\delta^{13}C$ values than those typifying zone II, but not as high as in zone I. The covariant isotopic trend of oxygen is not as pronounced as that of carbon.

4.3. Rare earth elements and trace elements

Rare earth element and trace element data are listed in Table 2. The ΣREE in seep carbonates are variable, ranging from 1.6 to 33.6 ppm in sample GeoB 8212-2a, 14.4–42.5 ppm in sample GeoB 8212-2b, 41.6 ppm in sample GeoB 8215-2c, and 23.2 ppm in sample GeoB 8212-2d. The ΣREE in sample GeoB 8212-2b is higher in the microcrystalline phase of zone II than in the peripheral microcrystalline phase of zone III (Fig. 7); the ΣREE in aragonite of the central zone I is lower than that of the microcrystalline phases (Table 2; Fig. 7). The shale-normalized REE of the studied seep carbonates are characterized by slight light REE (LREE) and heavy REE (HREE) depletion. All samples show pronounced and real positive Ce anomalies ($Ce/Ce^* > 1.3$; Figs. 8 and 9), suggesting precipitation under anoxic conditions. The Eu anomaly observed in four of the samples is most probably due to an interference with Ba oxides during ICP-MS analysis (Qi et al., 2005).

Strontium contents in carbonates range from 2462 ppm to 12,369 ppm and are higher in aragonite-rich subsamples (Table 2). Samples show Ba contents ranging from 86 ppm to 3372 ppm. Sample GeoB 8212-2a has the highest Ba content (3372 ppm), which is consistent with the detection of barite by XRD (Table 1). Contents of redox sensitive elements such as V, Mo, U, and Cd are highly variable. However, it appears that higher contents coincide with microcrystalline aragonite rather than fibrous aragonite or microcrystalline calcite (Table 2). With respect to sample GeoB 8212-2b, contents of V, Mo, U, and Cd are higher in microcrystalline phase of zone II than in the peripheral microcrystalline phase of zone III (Fig. 7); they are lowest in the central part of zone I (Fig. 7; Table 2).

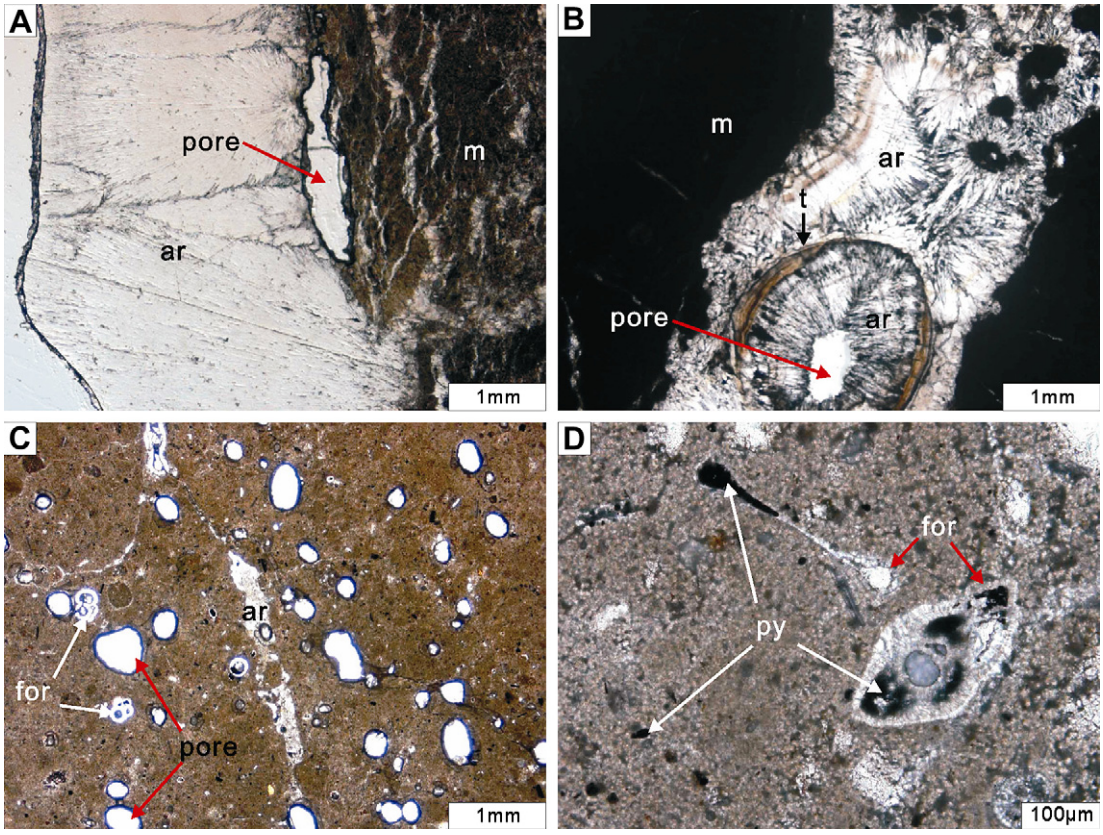

Fig. 2. Thin section photomicrographs of carbonate samples. (A) Acicular aragonite cement (ar) up to 5 mm in length postdating micrite (m); pore = pore space (black arrow); plane polarized light, GeoB 8212-2a. (B) Aragonite cement (ar) within microcrystalline calcite; the organic vestimentiferan tube (t) is surrounded and infilled by acicular aragonite (ar). Plane polarized light, GeoB 8212-2b. Carbonate mineralization directly associated with vestimentiferan tube is described elsewhere (Haas et al., 2009). (C) Pores (red arrows), approximately 0.5 mm in diameter and foraminifers ("for" with white arrows), are common; plane polarized light, GeoB 8215-2c. (D) Pyrite framboids ("py" white arrows) are dispersed within carbonate matrix and occur as infilling of foraminifer tests ("for" with red arrows). Plane polarized light, GeoB 8212-2a. (For interpretation of the references to colour in this figure legend, the reader is referred to the web version of this article).

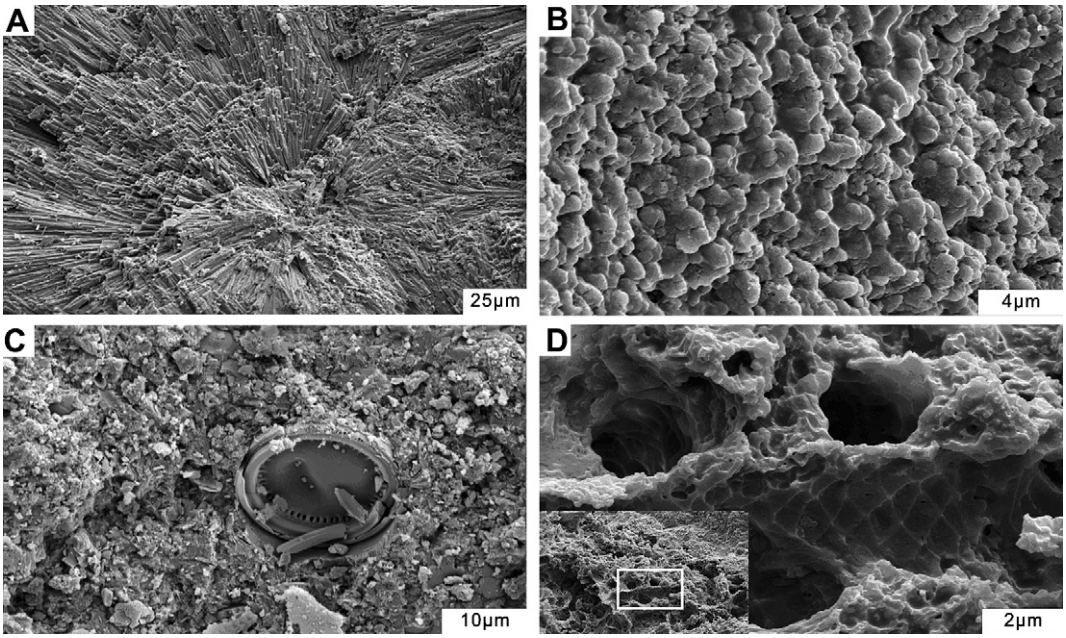

Fig. 3. Scanning electron micrographs of carbonate textures. Cement is represented by aragonite (A) and high-magnesium calcite (B), GeoB 8212-2a. (C) Well-preserved diatom in the carbonate matrix, GeoB 8212-2b. (D) Micropores in μm-size range, GeoB 8215-2c.

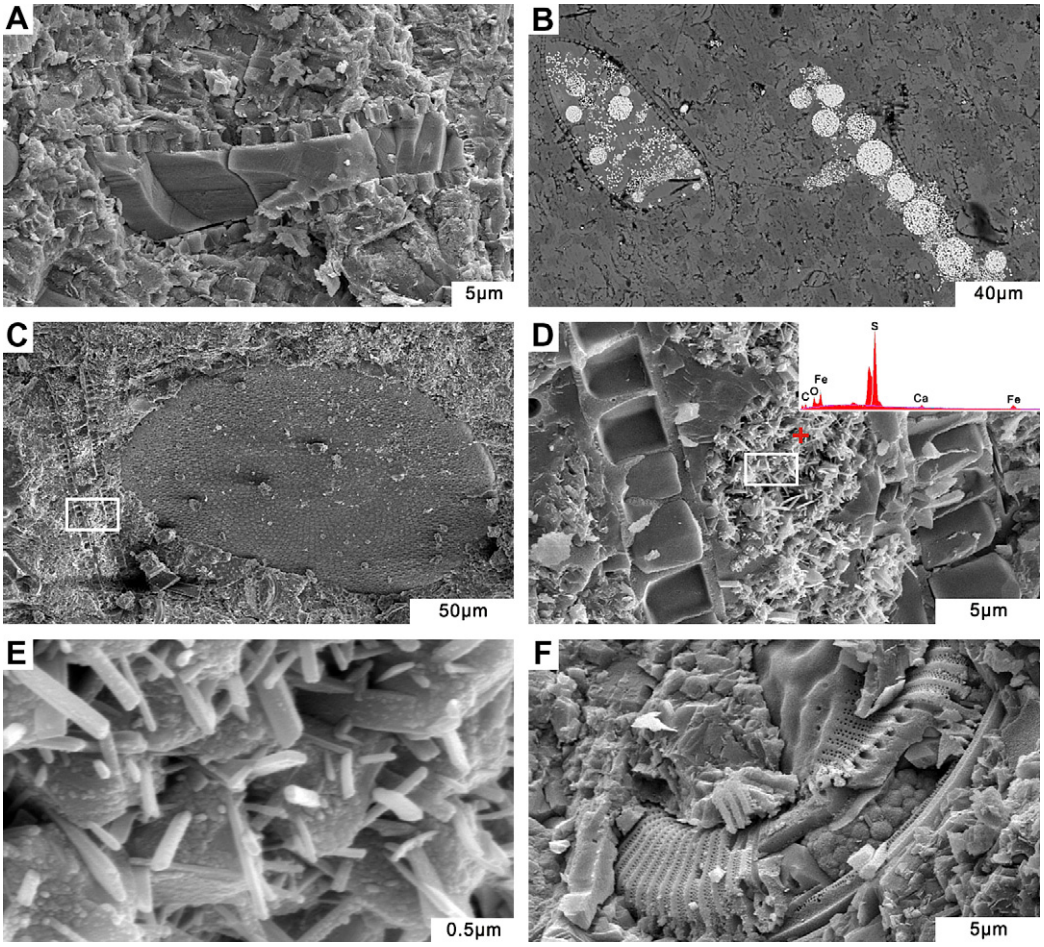

Fig. 4. Scanning electron micrographs of authigenic carbonates. (A) Well-preserved foraminifera, GeoB 8212-2b. (B) Pyrite framboids (white) occur as infilling of foraminifer tests. Back-scatter electron mode micrograph, GeoB 8212-2b. (C) Diatom (right) and foraminifera (left); the box inset shows location of photomicrograph (D), GeoB 8212-2d. (D) Pyrite and rod-shaped carbonate cement infilling foraminifer test. The energy dispersive spectrometry scans indicate the relative proportions of Fe, S, Ca, C, and O (dotted cross). (E) Enlargement representing the box in (D), showing pyrite and associated rod-shaped carbonate crystals. (F) Pyrite framboids infilling a diatom, GeoB 8215-2c.

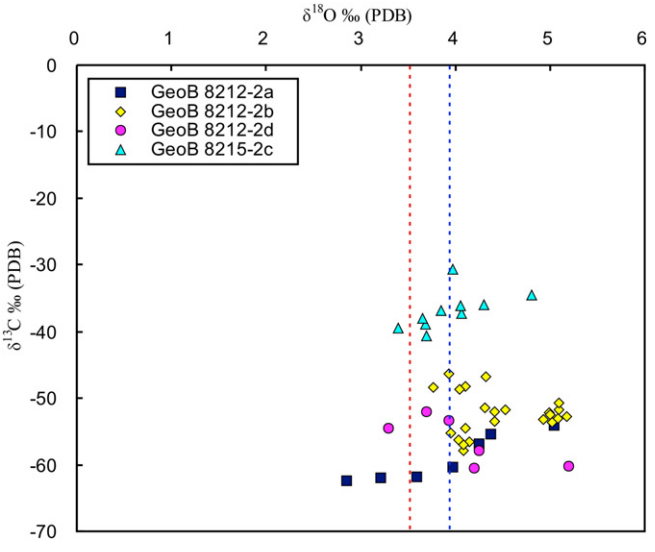

Fig. 5. Stable carbon and oxygen isotopic compositions of authigenic carbonates. The dashed lines indicate $\delta^{18}O$ values for aragonite (3.9‰; blue) and calcite (3.5‰; red) representing precipitation in equilibrium with bottom water at present temperature. (For interpretation of the references to colour in this figure legend, the reader is referred to the web version of this article).

5. Discussion

5.1. Composition of seepage fluids

The carbon isotopic composition of seep carbonates serves as an indicator of the carbon sources (e.g. Roberts and Aharon, 1994; Peckmann et al., 2001; Peckmann and Thiel, 2004; Naehr et al., 2007). Parent methane is usually significantly more depleted in ^{13}C than the resulting carbonate precipitates due to the incorporation of carbon from other sources than methane; assuming mixture of methane-derived carbonate ions and marine carbonate ions, typically not more than two-thirds of the carbon in seep carbonate minerals is derived from the former source (Peckmann and Thiel, 2004 and references therein). The strongly negative carbon isotope compositions of carbonates from Hydrate Hole ($\delta^{13}C$ values: −62.5‰ to −46.3‰; Fig. 5) thus indicate that the carbon source is mainly biogenic methane ($\delta^{13}C$ values of biogenic methane are <−50‰; Whiticar, 1999). The Diapir Field carbonate phases show higher $\delta^{13}C$ values (−40.7‰ to −30.7‰; Fig. 5). These values either reflect (1) parent methane, which is less depleted in ^{13}C than at Hydrate Hole, (2) relative enrichment of ^{13}C as a function of ongoing consumption of methane, or (3) a higher contribution of carbonate from other sources. Although, we are unable to exclude scenarios (2) and (3), the geological setting of the Diapir Field seep

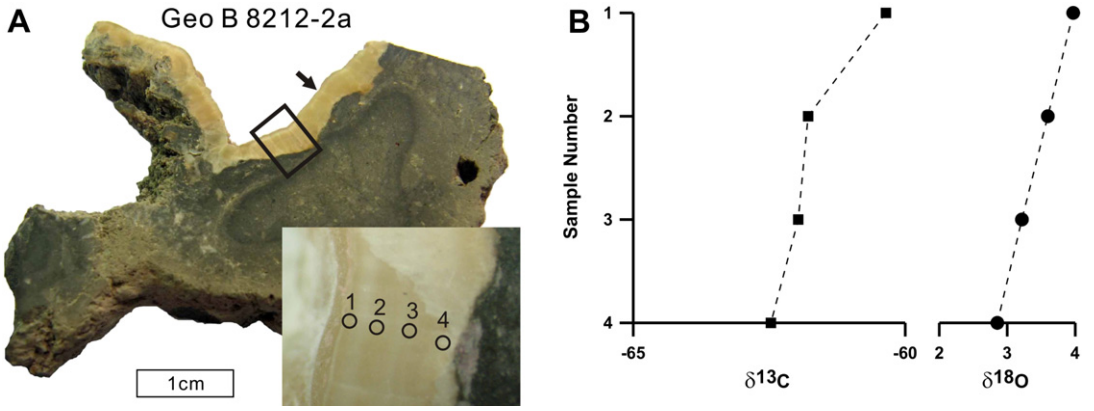

Fig. 6. (A) Photograph of sample GeoB 8212-2a, aragonite appears as yellowish layer (black arrow). The box inset shows the location of the image in lower right corner with indication of subsamples. (B) Plot of $\delta^{13}C$ and $\delta^{18}O$ data of subsamples in (A).

site accounts for methane deriving from deeper sources. At this site, seepage of methane-bearing fluids is probably due to the remobilization and alteration of hydrocarbons from the Late Aptian black shales and subsequent migration through the salt-diapir (cf. Emery et al., 1975). Buried for more than 2000 m, the Late Aptian black shales are mature enough to generate hydrocarbons (cf. Sahling et al., 2008). Thermogenic methane, usually generated in deeper horizons than biogenic methane, is typified by higher $\delta^{13}C$ values than biogenic methane ($\delta^{13}C$ values of thermogenic methane are $>-50‰$; Whiticar, 1999).

The $\delta^{18}O$ values, on the other hand, provide information pertaining to the temperature and fluid source from which seep carbonate precipitated (e.g. Naehr et al., 2000). Assuming precipitation of aragonite and calcite in equilibrium with bottom water at the present bottom water temperature, $\delta^{18}O$ values of 3.9‰ and 3.5‰ would be expected, respectively. These calculations differ

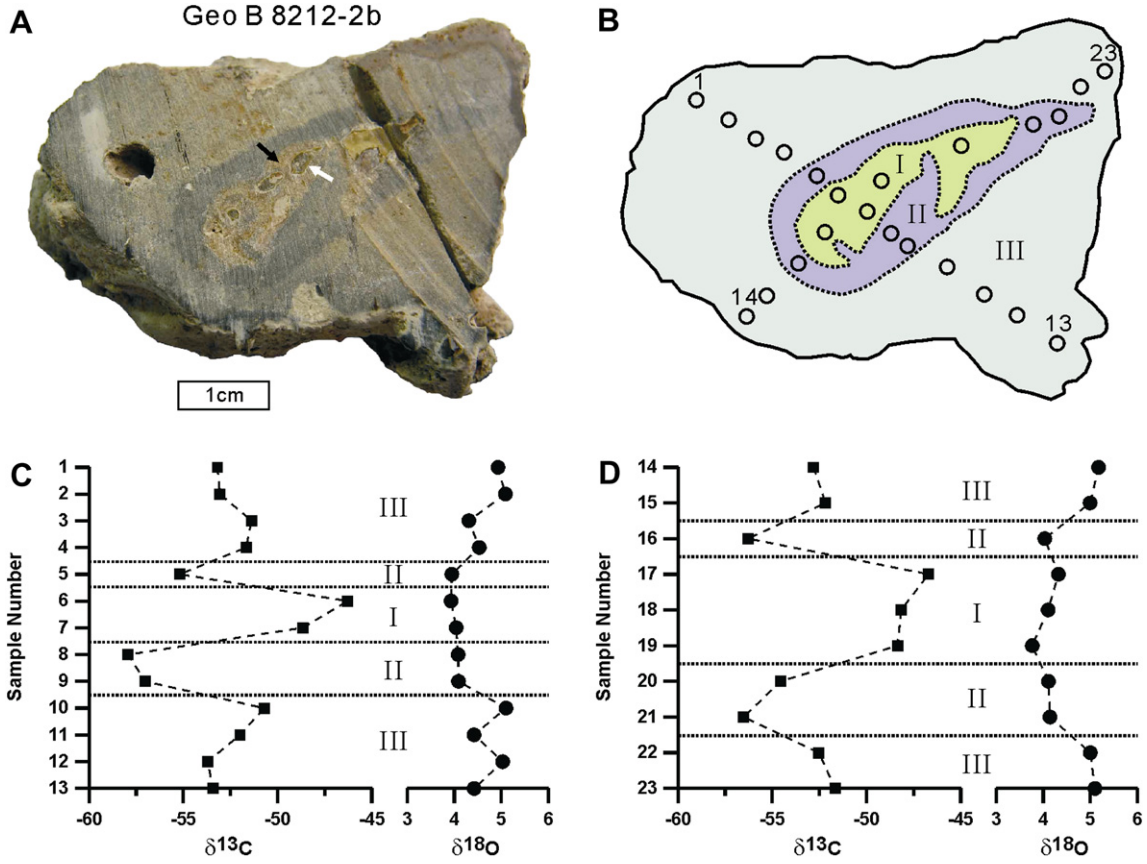

Fig. 7. (A) Photograph of laminated sample GeoB 8212-2b. Worm tube (white arrow) surrounded by pure aragonite cement (black arrow). (B) Drawing of the same sample with positions of subsamples indicated. (C) Plot of $\delta^{13}C$ and $\delta^{18}O$ data of subsamples 1–13; (D) Plot of $\delta^{13}C$ and $\delta^{18}O$ data of subsample numbers 14–23. Delineation of the three zones of distinct isotopic signatures (I to III) indicated in (C) and (D).

Table 2
Rare earth element and trace element contents (ppm; 5% HNO_3-treated solution) of authigenic carbonates.

Element	GeoB 8212-2a-1	GeoB 8212-2a-2	GeoB 8212-2a-3	GeoB 8212-2b-1	GeoB 8212-2b-2	GeoB 8212-2b-3	GeoB 8215-2c	GeoB 8212-2d
La	0.19	4.50	3.23	2.14	6.13	4.46	6.70	3.17
Ce	0.89	16.81	11.94	7.44	21.93	16.26	19.42	12.05
Pr	0.07	1.47	1.03	0.61	1.79	1.34	1.86	1.04
Nd	0.27	5.95	4.04	2.30	7.10	4.94	7.60	3.86
Sm	0.06	1.21	0.84	0.47	1.47	1.04	1.54	0.77
Eu	0.02	0.40	0.29	0.10	0.32	0.23	0.35	0.33
Gd	0.05	1.08	0.70	0.37	1.24	0.88	1.36	0.65
Tb	0.01	0.17	0.11	0.07	0.20	0.14	0.21	0.10
Dy	0.04	0.93	0.58	0.35	1.06	0.73	1.10	0.61
Ho	0.01	0.17	0.11	0.07	0.21	0.14	0.23	0.09
Er	0.02	0.44	0.28	0.20	0.54	0.38	0.61	0.25
Tm	<0.01	0.06	0.04	0.03	0.08	0.05	0.08	0.03
Yb	0.02	0.37	0.24	0.19	0.43	0.34	0.51	0.19
Lu	<0.01	0.05	0.03	0.03	0.07	0.05	0.08	0.03
ΣREE	1.64	33.60	23.46	14.36	42.54	30.99	41.64	23.17
Ce/Ce*	1.84	1.54	1.56	1.56	1.56	1.62	1.27	1.62
Pr/Pr*	0.87	0.86	0.87	0.86	0.84	0.86	0.90	0.89
Eu/Eu*	1.89	1.66	1.78	1.15	1.11	1.15	1.13	2.19
Sc	1.24	1.92	2.03	1.38	1.84	1.82	1.80	1.60
V	0.43	6.98	7.04	3.52	9.50	8.59	13.6	6.38
Cr	2.16	4.43	4.57	2.98	4.90	4.61	4.99	4.42
Co	1.56	1.84	2.00	1.59	1.65	1.59	1.70	1.77
Ni	8.17	8.64	11.9	12.2	7.58	6.90	7.15	8.05
Sr	12,369	5321	9465	8460	6878	3739	4814	2461
Y	0.51	3.94	2.64	1.97	4.92	3.35	5.24	2.11
Mo	0.61	1.71	2.15	1.68	4.42	3.04	3.25	1.35
Cd	0.12	0.12	0.22	0.15	0.32	0.30	0.23	0.50
Ba	3372	86	352	531	650	437	298	326
Th	0.01	1.40	1.08	0.46	1.41	1.02	1.00	0.74
U	1.92	4.10	4.31	5.26	14.7	14.4	10.2	4.94

GeoB 8212-2a-1 is pure aragonite rim. GeoB 8212-2b-1, GeoB 8212-2b-2, and GeoB 8212-2b-3 were collected from zones I, zone II, and zone III, respectively, as indicated in Fig. 7. GeoB 8212-2a-2, GeoB 8212-2d, and GeoB 8215-2c are bulk samples.

slightly from the measured average $\delta^{18}O$ values (2.9‰–5.2‰ for Hydrate Hole samples, and 3.4‰ to 4.8‰ for Diapir Field sample; Fig. 5). Due to the enrichment of ^{18}O in gas hydrates, anomalously positive $\delta^{18}O$ of seep carbonate are often taken as an argument for gas hydrate destabilization at seeps (Bohrmann et al., 1998; Aloisi et al., 2000; Greinert et al., 2001; Peckmann and Thiel, 2004; Chen et al., 2005). The smectite-illite transition in deep sediments can also generate ^{18}O-enriched pore water (Hesse, 2003). Because gas hydrate bearing sediments have been found in depths greater than 0.5 m at the study sites (Sahling et al., 2008), decomposition of gas hydrate is the most likely mechanism responsible for ^{18}O enrichment. The few unusually low $\delta^{18}O$ values (as low as 2.9‰) of the studied carbonates may result from the episodical expulsion of warm fluids, which already has been reported elsewhere, for example in the Gulf of Mexico (Roberts, 2001).

5.2. Microbial mediation of carbonate precipitation

Evidence for an involvement of microbes in the formation of seep carbonates derives from stable isotopes, biomarkers, and biogenic fabrics. It has been demonstrated that consortia of MOA and SRB are responsible for the oxidation of methane and subsequent formation of authigenic carbonates at seeps (e.g. Hinrichs et al., 1999; Boetius et al., 2000; Peckmann and Thiel, 2004; Campbell, 2006). The carbonate carbon isotope values (as low as −62.5‰; Fig. 5) of the Congo fan seep carbonates are too low to be explained by carbon sources other than methane (cf. Whiticar, 1999; Naehr et al., 2007), indicating that they derived from AOM mediated by microbes.

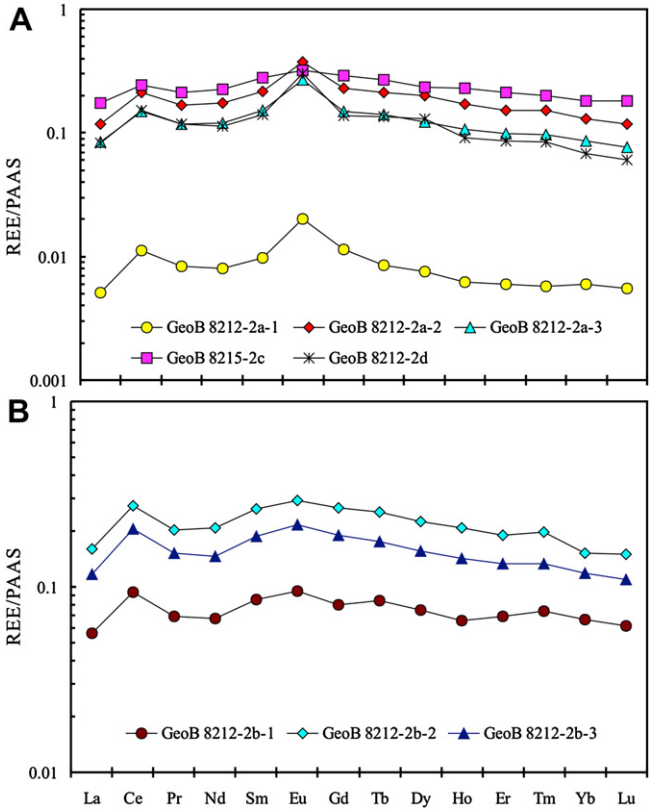

Fig. 8. Shale-normalized REE patterns of seep carbonates measured as 5% HNO_3-treated solutions. (A) Samples GeoB 8212-2a, GeoB 8212-2d, and GeoB 8215-2c; (B) Sample GeoB 8212-2b.

We detected abundant putative microbial textures in the carbonates. Among them are pyrite framboids found in the tests of foraminifera (Figs. 2D and 4B–F). Similar framboidal textures have been found in other modern seep carbonates (Kohn et al., 1998; Naehr et al., 2000; Díaz-del-Río et al., 2003; Feng et al., 2008). The rod-shaped habit of carbonate cement found in some foraminiferal tests enclosed in the Congo fan seep carbonates (Fig. 4C–E) is obviously not an unambiguous criterion for a microbial origin. But interestingly, rod-shaped habits have been found to be particular

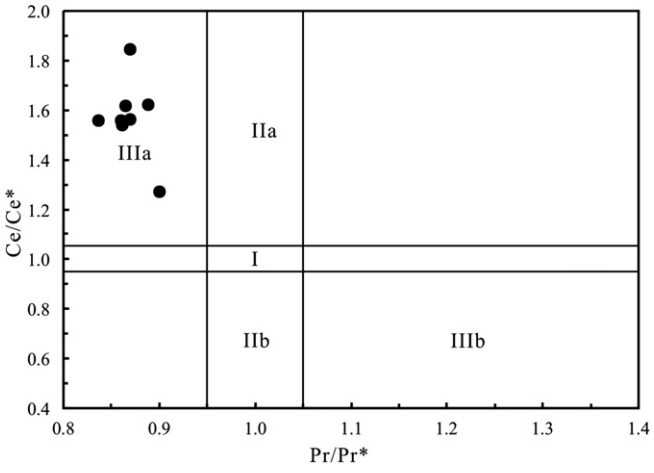

Fig. 9. Plot of Ce/Ce* vs. Pr/Pr* (after Bau and Dulski, 1996). Field I: no anomaly; Field IIa: positive La anomaly, no Ce anomaly; Field IIb: negative La anomaly, no Ce anomaly; Field IIIa: real positive Ce anomaly; Field IIIb: real negative Ce anomaly. All samples show real positive Ce anomalies suggesting precipitation under anoxic conditions.

abundant among microbial carbonates (Verrecchia and Verrecchia, 1994; Chafetz et al., 1998; Peckmann et al., 1999), including seep carbonates (e.g. Han et al., 2008). Han et al. (2008) reported two kinds of rod-shaped crystals, one with square terminations and another with rounded terminations: both were suggested to be of microbial origin. The rod-shaped crystals detected in our samples show square ends and coexist with pyrite framboids (Fig. 4D–E).

5.3. Control of seepage rate on carbonate formation

Seafloor observations reveal that both physical and chemical characteristics of seep environments are highly variable (Roberts, 2001; Tryon and Brown, 2004; Solomon et al., 2008). This variability is responsible for the creation of unique seafloor features (Roberts and Carney, 1997; Roberts, 2001; Hovland, 2002; León et al., 2007; Lapham et al., 2008). The depth in which methane is oxidized in sediments at seeps is mostly a function of fluid flow intensity, with higher intensities leading to a shallower oxidation zone or even partial methane flux into the bottom water (Treude et al., 2003; Luff et al., 2005). Temporal variability of upward fluid flux has been documented by successive shifts in isotopic composition of authigenic carbonate phases precipitated at seeps (De Boever et al., 2006a,b). Permeability and fluid flow are diminished by the formation of authigenic carbonate phases, clogging the pore space of surface sediments. These modifications influence both mineralogy and isotopic signature of the seep carbonates forming subsequently (Luff et al., 2005; Bayon et al., 2009).

All shale-normalized REE patterns of the Congo fan seep carbonates display positive Ce anomalies ($Ce/Ce^* > 1.3$; Fig. 8), confirming precipitation under anoxic conditions. The REE and trace element patterns of seep carbonates reflect a mixture between seep fluids and seawater. It is widely accepted that V, Mo, U, and Cd are redox sensitive elements that become enriched under anoxic conditions (Morford and Emerson, 1999). It also has been suggested that REE contents decrease slightly after an initial increase at shallow depths below the seafloor due to reduction of Fe-oxides (Haley et al., 2004; Elderfield and Sholkovitz, 1987). Redox conditions at seeps are presumed to be closely related to the flux of fluids (cf. De Boever et al., 2006a,b; Feng et al., 2009a,b). Accordingly, temporal variability in fluid flux is likely to be archived in REE and trace element contents of authigenic carbonates.

Sample GeoB 8212-2b shows concentric lamination, corresponding to fluctuations in $\delta^{13}C$ values (Fig. 7) and variable REE and trace elements contents with low $\delta^{13}C$ values correlating with high REE contents (Fig. 8 and Table 2). We suggest that the flux intensity of seep fluids is one factor that controls this kind of variability. During times of relatively slow seepage, methane was probably oxidized deeper below the sediment/water interface, which resulted in the low $\delta^{13}C_{carbonate}$ values of Zone II (Fig. 7) due to fewer admixtures of marine carbonate ions. Under these more reducing conditions, carbonates presumably incorporated more REE and trace elements (Table 2 and Fig. 8). In contrast, during times of relatively high fluxes, methane oxidation occurred closer to the sediment/water interface (cf. De Boever et al., 2006a,b), which resulted in higher $\delta^{13}C$ values and lower REE contents (Zone I in Fig. 7, Table 2 and Fig. 8) due to a stronger influence of marine waters. There is no direct evidence for gas flow at the Congo fan seeps such as bubbles escaping from the seafloor or acoustic anomalies in the water column (Sahling et al., 2008). However, it has been suggested that gas flows are probably transient events (Sahling et al., 2008). The observations made in this study are in good accordance with the concept of transient gas flow. Our data consequently suggest that the heterogeneity observed in seep carbonates results at least partly from temporal variations of methane flux intensity.

6. Conclusions

Authigenic carbonates collected from the seep sites Hydrate Hole and Diapir Field of the northern Congo deep-sea fan mainly consist of aragonite and high-Mg calcite. Microbial textures recognized in these carbonates include rod-shaped carbonate crystals and framboidal pyrite both also infilling foraminiferal tests. Low $\delta^{13}C_{carbonate}$ values (as low as $-62.5‰$) indicate that the carbon source was mainly methane. Enrichment of ^{18}O in some carbonate phases ($\delta^{18}O$ values as high as $5.2‰$) is probably related to destabilization of gas hydrates in the underlying sediments, while unusually low $\delta^{18}O$ values (as low as $2.9‰$) of other phases may result from higher temperature possibly related to episodical expulsion of warmer fluids. A sample with concentric lamination from Hydrate Hole is suggested to archive varying seepage conditions reflected in the laminated fabric with changing stable isotopic and elemental signatures. During relatively slow seepage, methane was presumably oxidized relatively deep below the sediment/water interface under strictly reducing conditions documented by high REE and trace element contents. In contrast, during times of relatively high flux, seepage likely forced methane closer to the seafloor where it was oxidized under less reducing conditions, reflected by lower REE and trace element contents.

Acknowledgments

This study was partially supported by 973 Program (2009CB219506) and the NSF of China (Grants: 40725011 and U0733003). Dr. G.F. Xu (CSU) helped with FE-SEM analyses, Dr. Z. Li (CSU) with XRD analyses, Dr. J.X. Zhu (GIGCAS) with quantification of XRD results, Dr. W.F. Deng (GIGCAS) with isotope analyses, and Dr. L. Qi (IGCAS) with the analyses of REE and trace elements. Additional financial support was provided by the "Deutsche Forschungsgemeinschaft" through the DFG-Excellence Cluster MARUM, Bremen. We appreciate the thoughtful and constructive comments provided by associate editor Prof. A. Aplin, Dr. G. Bayon, and an anonymous reviewer, which improved the manuscript. This is contribution No. IS-1095 from GIGCAS.

References

Aloisi, G., Pierre, C., Rouchy, J.M., Foucher, J.P., Woodside, J., 2000. Methane-related authigenic carbonates of eastern Mediterranean Sea mud volcanoes and their possible relation to gas hydrate destabilisation. Earth and Planetary Science Letters 184, 321–338.

Bau, M., Dulski, P., 1996. Distribution of yttrium and rare-earth elements in the Penge and Kuruman iron-formations, Transvaal Supergroup, South Africa. Precambrian Research 79, 37–55.

Bayon, G., Henderson, G.M., Bohn, M., 2009. U-Th stratigraphy of a cold seep carbonate crust. Chemical Geology 260, 47–56.

Berner, R.A., 1980. Early Diagenesis – a Theoretical Approach. Princeton University Press, Princeton.

Birgel, D., Peckmann, J., 2008. Aerobic methanotrophy at ancient marine methane seeps: a synthesis. Organic Geochemistry 39, 1659–1667.

Boetius, A., Ravenschlag, K., Schubert, C.J., Rickert, D., Widdel, F., Gieseke, A., Amann, R., Jørgensen, B.B., Witte, U., Pfannkuche, O., 2000. A marine microbial consortium apparently mediating anaerobic oxidation of methane. Nature 407, 623–626.

Bohrmann, G., Greinert, J., Suess, E., Torres, M., 1998. Authigenic carbonates from the Cascadia subduction zone and their relation to gas hydrate stability. Geology 26, 647–650.

Campbell, K.A., 2006. Hydrocarbon seep and hydrothermal vent paleoenvironments and paleontology: past developments and future research directions. Palaeogeography, Palaeoclimatology, Palaeoecology 232, 362–407.

Castellini, D.G., Dickens, G.R., Snyder, G.T., Ruppel, C.D., 2006. Barium cycling in shallow sediment above active mud volcanoes in the Gulf of Mexico. Chemical Geology 226, 1–30.

Chafetz, H.S., Akdim, B., Julia, R., Reid, A., 1998. Mn- and Fe-rich black travertine shrubs: bacterially (and nanobacterially) induced precipitates. Journal of Sedimentary Research 68, 404–412.
Chen, D.F., Cathles, L.M., Roberts, H.H., 2004. The geochemical signatures of variable gas venting at gas hydrate sites. Marine and Petroleum Geology 21, 317–326.
Chen, D.F., Huang, Y.Y., Yuan, X.L., Cathles, L.M., 2005. Seep carbonates and preserved methane oxidizing archaea and sulfate reducing bacteria fossils suggest recent gas venting on the seafloor in the Northeastern South China Sea. Marine and Petroleum Geology 22, 613–621.
Chen, D.F., Feng, D., Su, Z., Song, Z.G., Chen, G.Q., Cathles, L.M., 2006. Pyrite crystallization in seep carbonates at gas vent and hydrate site. Materials Science and Engineering: C 26, 602–605.
Chen, D.F., Liu, Q., Zhang, Z.W., Cathles, L.M., Roberts, H.H., 2007. Biogenic fabrics in seep carbonates from an active gas vent site in Green Canyon Block 238, Gulf of Mexico. Marine and Petroleum Geology 24, 313–320.
De Boever, E., Swennen, R., Dimitrov, L., 2006a. Lower Eocene carbonate cemented chimneys (Varna, NE Bulgaria): formation mechanisms and the (a)biological mediation of chimney growth? Sedimentary Geology 185, 159–173.
De Boever, E., Swennen, R., Dimitrov, L., 2006b. Lower Eocene carbonate-cemented "chimney" structures (Varna, Bulgaria) – control of seepage rates on their formation and stable isotopic signature. Journal of Geochemical Exploration 89, 78–82.
Díaz-del-Río, V., Somoza, L., Martínez-Frias, J., Mata, M.P., Delgado, A., Hernandez-Molina, F.J., Lunar, R., Martín-Rubí, J.A., Maestro, A., FernándezPuga, M.C., Leon, R., Llave, E., Medialdea, T., Vázquez, J.T., 2003. Vast fields of hydrocarbon-derived carbonate chimneys related to the accretionary wedge/olistostrome of the Gulf of Cádiz. Marine Geology 195, 177–200.
Droz, L., Rigaut, F., Cochonat, P., Tofani, R., 1996. Morphology and recent evolution of the Zaire turbidite system (Gulf of Guinea). Geological Society of America Bulletin 108, 253–269.
Elderfield, H., Sholkovitz, E.R., 1987. Rare earth elements in the pore waters of reducing nearshore sediments. Earth and Planetary Science Letters 82, 280–288.
Emery, K.O., Uchupi, E., Phillips, J., Bowin, C., Mascle, J., 1975. Continental margin off Western Africa: Angola to Sierra Leone. American Association of Petroleum Geologists Bulletin 59, 2209–2265.
Feng, D., Chen, D.F., Roberts, H.H., 2008. Sedimentary fabrics in the authigenic carbonates from Bush Hill: implication for seabed fluid flow and its dynamic signature. Geofluids 8, 301–310.
Feng, D., Chen, D.F., Peckmann, J., 2009a. Rare earth elements in seep carbonates as tracers of variable redox conditions at ancient hydrocarbon seeps. Terra Nova 21, 49–56.
Feng, D., Chen, D.F., Roberts, H.H., 2009b. Petrographic and geochemical characterization of seep carbonate from Bush Hill (GC 185) gas vent and hydrate site of the Gulf of Mexico. Marine and Petroleum Geology 26, 1190–1198.
Gay, A., Lopez, M., Ondreas, H., Charlou, J.L., Sermondadaz, G., Cochonat, P., 2006a. Seafloor facies related to upward methane flux within a Giant Pockmark of the Lower Congo Basin. Marine Geology 226, 81–95.
Gay, A., Lopez, M., Cochonat, P., Séanne, M., Levaché, D., Sermondadaz, G., 2006b. Isolated seafloor pockmarks linked to BSRs, fluid chimneys, polygonal faults and stacked Oligocene-Miocene turbiditic palaeochannels in the Lower Congo Basin. Marine Geology 226, 25–40.
Greinert, J., Bohrmann, G., Suess, E., 2001. Gas hydrate-associated carbonates and methane-venting at Hydrate Ridge: classification, distribution, and origin of authigenic lithologies. In: Paull, C.K., Dillon, W.P. (Eds.), Natural Gas Hydrates: Occurrence, Distribution and Detection. Geophysical Monograph, vol. 124. American Geophysical Union, Washington, DC, pp. 131–143.
Haas, A., Little, C.T.S., Sahling, H., Bohrmann, G., Himmler, T., Peckmann, J., 2009. Mineralization of vestimentiferan tubes at methane seeps on the Congo deep-sea fan. Deep Sea Research Part I: Oceanographic Research Papers 56, 283–293.
Han, X.Q., Suess, E., Huang, Y.Y., Wu, N.Y., Bohrmann, G., Su, X., Eisenhauer, A., Rehder, G., Fang, Y.X., 2008. Jiulong methane reef: microbial mediation of seep carbonates in the South China Sea. Marine Geology 249, 243–256.
Haley, B.A., Klinkhammer, G.P., McManus, J., 2004. Rare earth elements in pore waters of marine sediments. Geochimica et Cosmochimica Acta 68, 1265–1279.
Hesse, R., 2003. Pore water anomalies of submarine gas-hydrate zone as tool to assess hydrate abundance and distribution in subsurface: what have we learned in the past decade? Earth-Science Reviews 61, 149–179.
Hinrichs, K.-U., Hayes, J.M., Sylva, S.P., Brewer, P.G., DeLong, E.F., 1999. Methane-consuming archaebacteria in marine sediments. Nature 398, 802–805.
Hovland, M., 2002. On the self-sealing nature of marine seeps. Continental Shelf Research 22, 2387–2394.
Kohn, M.J., Riciputi, L.R., Stakes, D., Orange, D.L., 1998. Sulfur isotope variability in biogenic pyrite: reflections of heterogeneous bacterial colonization? American Mineralogist 83, 1454–1468.
Lapham, L.L., Chanton, J.P., Martens, C.S., Sleeper, K., Woolsey, J.R., 2008. Microbial activity in surficial sediments overlying acoustic wipeout zones at a Gulf of Mexico cold seep. Geochemistry Geophysics Geosystems 9, Q06001. doi:10.1029/2008GC001944.
León, R., Somoza, L., Medialdea, T., González, F., Díaz-del-Río, V., Fernández-Puga, M., Maestro, A., Mata, M., 2007. Sea-floor features related to hydrocarbon seeps in deepwater carbonate-mud mounds of the Gulf of Cádiz: from mud flows to carbonate precipitates. Geo-Marine Letters 27, 237–247.
Luff, R., Greinert, J., Wallmann, K., Klaucke, I., Suess, E., 2005. Simulation of long-term feedbacks from authigenic carbonate crust formation at cold vent sites. Chemical Geology 216, 157–174.
Marton, L.G., Tari, G.C., Lehmann, C.T., 2000. Evolution of the Angola passive margin, West Africa, with emphasis on post-salt structural styles. In: Moriak, W., Talwani, W. (Eds.), Atlantic Rifts and Continental Margins. Geophysical Monograph, vol. 115. American Geophysical Union, Washington, DC, pp. 129–149.
McArthur, J.M., Walsh, J.N., 1984. Rare-earth geochemistry of phosphorites. Chemical Geology 47, 191–220.
McLennan, S.M., 1989. Rare earth elements in sedimentary rocks: influence of provenance and sedimentary processes. In: Lipin, B.R., McKay, G.A. (Eds.), Geochemistry and Mineralogy of Rare Earth Elements. Reviews in Mineralogy, vol. 21, pp. 169–200.
Morford, J.L., Emerson, S., 1999. The geochemistry of redox sensitive trace metals in sediments. Geochimica et Cosmochimica Acta 63, 1735–1750.
Naehr, T.H., Rodriguez, N.M., Bohrmann, G., Paull, C.K., Botz, R., 2000. Methane derived authigenic carbonates associated with gas hydrate decomposition and fluid venting above the Blake Ridge Diapir. In: Paull, C.K., Matsumoto, R., Wallace, P.J., Dillon, W.P. (Eds.), Proceedings of the Ocean Drilling Program, Scientific Results, vol. 164, pp. 285–300.
Naehr, T.H., Eichhubl, P., Orphan, V.J., Hovland, M., Paull, C.K., Ussler III, W., Lorenson, T.D., Greene, H.G., 2007. Authigenic carbonate formation at hydrocarbon seeps in continental margin sediments: a comparative study. Deep Sea Research Part II: Topical Studies in Oceanography 54, 1268–1291.
Pape, T., Blumenberg, M., Seifert, R., Egorov, V.N., Gulin, S.B., Michaelis, W., 2005. Lipid geochemistry of methane-seep-related Black Sea carbonates. Palaeogeography, Palaeoclimatology, Palaeoecology 227, 31–47.
Peckmann, J., Paul, J., Thiel, V., 1999. Bacterially mediated formation of diagenetic aragonite and native sulfur in Zechstein carbonates (Upper Permian, Central Germany). Sedimentary Geology 126, 205–222.
Peckmann, J., Reimer, A., Luth, U., Luth, C., Hansen, B.T., Heinicke, C., Hoefs, J., Reitner, J., 2001. Methane-derived carbonates and authigenic pyrite from the northwestern Black Sea. Marine Geology 177, 129–150.
Peckmann, J., Thiel, V., 2004. Carbon cycling at ancient methane-seeps. Chemical Geology 205, 443–467.
Qi, L., Zhou, M., Malpas, J., Sun, M., 2005. Determination of rare earth elements and Y in ultramafic rocks by ICP-MS after preconcentration using $Fe(OH)_3$ and $Mg(OH)_2$ coprecipitation. Geostandards and Geoanalytical Research 29, 131–141.
Roberts, H.H., Aharon, P., 1994. Hydrocarbon-derived carbonate buildups of the northern Gulf of Mexico continental slope: a review of submersible investigations. Geo-Marine Letters 14, 135–148.
Roberts, H.H., Carney, R.S., 1997. Evidence of episodic fluid, gas, and sediment venting on the northern Gulf of Mexico continental slope. Economic Geology 92, 863–879.
Roberts, H.H., 2001. Fluid and gas expulsion on the Northern Gulf of Mexico continental slope: mud-prone to mineral-prone responses. In: Paull, C.K., Dillon, W.P. (Eds.), Natural Gas Hydrates: Occurrence, Distribution, and Detection. American Geophysical Union, Washington, DC, pp. 145–161.
Sahling, H., Bohrmann, G., Spiess, V., Bialas, J., Breitzke, M., Ivanov, M., Kasten, S., Krastel, S., Schneider, R., 2008. Pockmarks in the Northern Congo fan area, SW Africa: complex seafloor features shaped by fluid flow. Marine Geology 249, 206–225.
Sholkovitz, E., Shen, G.T., 1995. The incorporation of rare earth elements in modern coral. Geochimica et Cosmochimica Acta 59, 2749–2756.
Shields, G.A., Webb, G.E., 2004. Has the REE composition of seawater changed over geological time? Chemical Geology 204, 103–107.
Solomon, E.A., Kastner, M., Jannasch, H., Robertson, G., Weinstein, Y., 2008. Dynamic fluid flow and chemical fluxes associated with a seafloor gas hydrate deposit on the northern Gulf of Mexico slope. Earth and Planetary Science Letters 270, 95–105.
Taylor, J.C., 1991. Computer programs for standardless quantitative analysis of minerals using the full powder diffraction profile. Powder Diffraction 6, 2–9.
Thiel, V., Peckmann, J., Seifert, R., Wehrung, P., Reitner, J., Michaelis, W., 1999. Highly isotopically depleted isoprenoids: molecular markers for ancient methane venting. Geochimica et Cosmochimica Acta 63, 3959–3966.
Treude, T., Boetius, A., Knittel, K., Wallmann, K., Jørgensen, B.B., 2003. Anaerobic oxidation of methane above gas hydrates at Hydrate Ridge, NE Pacific Ocean. Marine Ecology Progress Series 264, 1–14.
Tryon, M.D., Brown, K.M., 2004. Fluid and chemical cycling at Bush Hill: implications for gas- and hydrate-rich environments. Geochemistry Geophysics Geosystems 5, Q12004. doi:10.1029/2004GC000778.
Uenzelmann-Neben, G., 1998. Neogene sedimentation history of the Congo fan. Marine and Petroleum Geology 15, 635–650.
Valentine, D.L., Reeburgh, W.S., 2000. New perspectives on anaerobic methane oxidation. Environmental Microbiology 2 (5), 477–484.
Verrecchia, E.P., Verrecchia, K.E., 1994. Needle-fiber calcite: a critical review and a proposed classification. Journal of Sedimentary Research A64, 650–664.
Whiticar, M.J., 1999. Carbon and hydrogen isotope systematics of bacterial formation and oxidation of methane. Chemical Geology 161, 291–314.
Wright, J., Schrader, H., Holser, W.T., 1987. Paleoredox variations in ancient oceans recorded by rare earth elements in fossil apatite. Geochimica et Cosmochimica Acta 51, 631–644.